Topology-Directed Synthesis of Helical Phosphoniums with High Diradical Character and Polar-Dependent Electron Transfer

Bo Yang[1], Suqiong Yan[1], Shirong Ban[1], Yuan Zhang[1], Hui Ma[1], and Wei Huang[1,2]*

Molecular topology synthesis of polycyclic aromatic heterocycles (PAHs) with diradical character takes root in the intramolecular coupling breakthrough. Herein, we report selectively Mn(III)/Cu(II)-mediated C–P and C–H bond cleavage to obtain robust donor-fused phosphoniums with helical or planar geometries and distinct cationic charges. The former helical structures incorporate a common phospha[5]helication acceptor and different arylamines donors, and the latter planar one contains a phospha[6]dication and the same donors. These unprecedented donor-acceptor (D–A) pairs show unique topology-dependent optoelectronic properties. The folded helical radical centers possess an extreme electron-deficient state and through-space isolation with high diradical character (y_0 = 0.989). Moreover, the ingenious charge transfer (CT) and locally excited (LE) transition components facilitate diverse hybridized local and charge transfer (HLCT) in different solvents, endowing the highest emission bandgap variation of 0.78 eV (~217 nm). The cationic emission could also be adjusted from blue to near-infrared regions via topology tailoring and polar-dependent HLCT, which could output additional circularly polarized luminescence in a compatible chiral menthol matrix with elevated quantum efficiency and retained deep-red glow. It is worth mentioning that an atomically precise Mn(III) halide has been unprecedentedly captured and determined for the C–P bond activation.

INTRODUCTION

Developing intramolecular coupling protocol has received widespread applications in hierarchical topology control synthesis of photo-electro-magnetic PAHs through delocalized π-extension and spatial dimension upgrading in recent years.[1–7] Among them, heteroatom insertion is an attractive tactic to alter their geometries and electronic configurations. For instance, the C–C and C–N coupling almost uses [Pd]/[Ni]-catalytic intermolecular or intramolecular annulation to promote the delocalization.[8–12] The delocalization of electrons could possess diverse interaction processes via through-bond transfer (TBC) or through-space transfer (TSC) to create the topology dependence of the optoelectronic properties,[13–15] such as π-conjugated macrocycles,[16–19] nanographenes,[20–24] organic cages,[24,25] heteroatom doped PAHs,[27,28] and helicenes.[28–34]

Helicenes, the ortho-fused superstructures, have an intrinsic folded spiral superposition of PAHs.[36,37] The topology tailoring in helicenes endows an accessional possibility of stable radical incubation,[34,35,38] circularly polarized luminescence (CPL),[14,39,40] and chirality-induced spin selectivity (CISS).[41,42] The traditional carbon[*n*]helicenes with high diradical character and dynamic luminescence switchability is hardly accessible due to resonance delocalization and monotonous electron transfer inherency (*e.g.* typical π–π*), which gives rise to closed-shell species or inflexible emission at ambient conditions.[35,43–45] Generally, the stabilization of cationic radicals requires an electron-rich neutral nucleus to relax their reactive spots of electron-deficient radicals in a fully π-conjugated system via the TBC channel.[4,46] In this condition, the substituent protection is also required in many cases.[47] As a consequence, the stable diradical cations are exclusively produced from neutral electron-rich precursors (*e.g.,* neutral polythiophene and polyarylamine backbones). In contrast, through-space transfer (TSC) refers to weak interactions between two potential non-covalent contact units, which is highly dependent on the contact distance and D–A orientation.[48] Indeed, this landscape has been widely explored in a light-triggered excited state in TSC-type thermally activated delayed fluorescence (TADF).[15,49–52] Nevertheless, the potential intramolecular TSC via orbital coupling of the helical radicals has rarely been investigated up to now.[17,34] This TSC process might offset the drastic electron-deficient bridge to stabilize the diradicals but also enable expectant D–A character of the parent structures, which will provide additional topology-dependent photo-electro-magnetic properties as well. Unfortunately, ultra-strong D–A configurations with ionic pairs are still unexplored in this area, which is mainly due to the scanty synthetic methodology.

Based on this proof of concept, we develop a new type of electron-deficient helicenes from the main-group phosphine substrates by virtue of optimized Mn(III)-

[1]State Key Laboratory of Coordination Chemistry, Nanjing National Laboratory of Microstructures, School of Chemistry and Chemical Engineering, Nanjing University, Nanjing 210093, P. R. China. E-mail: whuang@nju.edu.cn

[2]Shenzhen Research Institute of Nanjing University, Shenzhen 518057, P. R. China

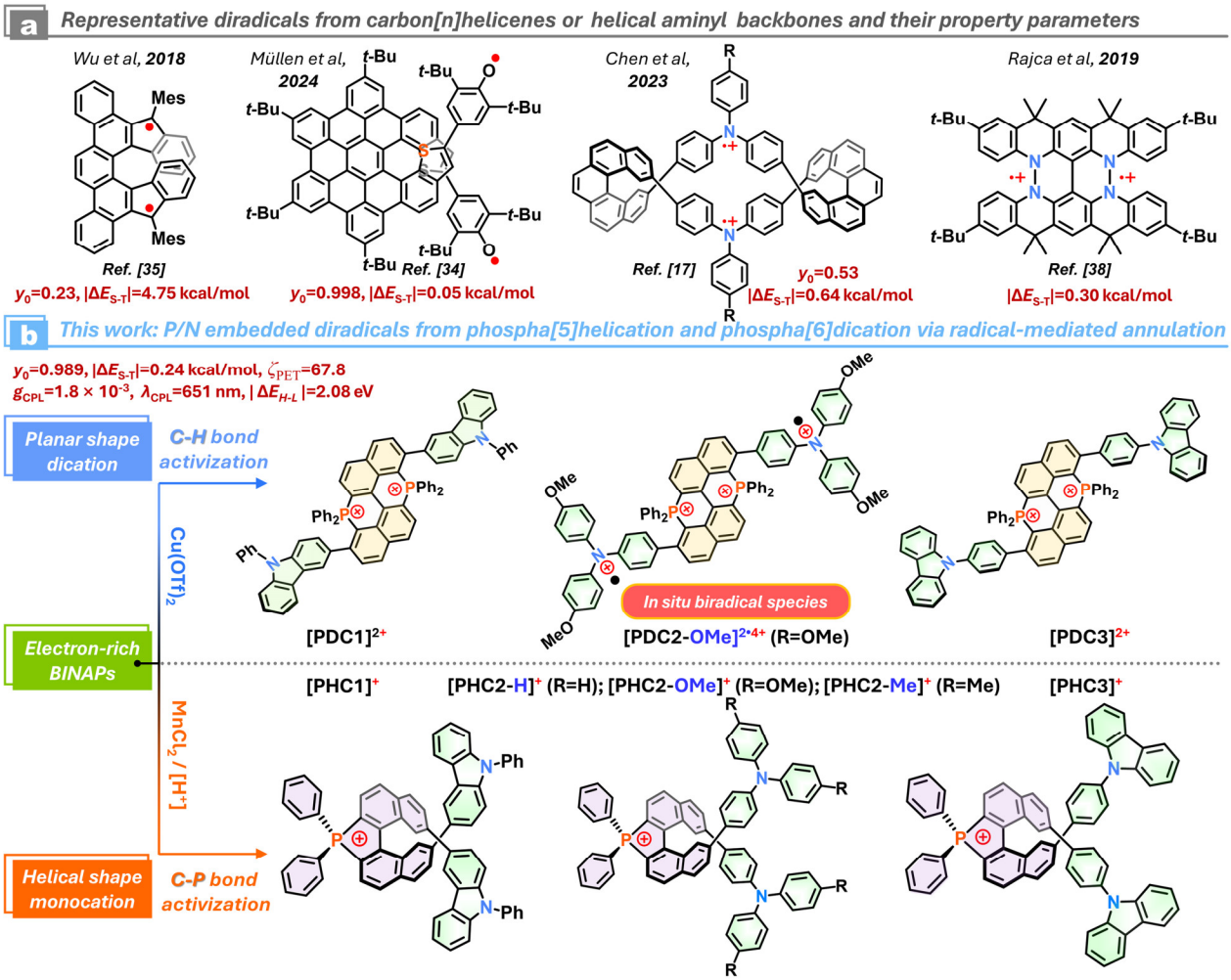

Figure 1. (a) Representative diradical helicenes in previous progresses. (b) Synthesis methodology and property parameters of helical and planar phosphoniums by Mn(III) and Cu(II)-mediated radical annulation.

mediated C−P bond cyclization, where the substrates carry electron-rich carbazole or triphenylamine groups. Although competitive single-electron oxidation might exist between *N* and *P* atoms, the first single-electron oxidation (SET) event proceeds on the P(III)-atom via the coordination assistance, generating a helical phosphonium core with extreme electron deficiency. Thus, the helical D−A phosphoniums with diverse HLCT and fluorescence switches are built ($\Delta\lambda_{em}$ up to 0.78 eV). The further SET oxidation of phosphonium by $AgSbF_6$ affords ammonium trications with high diradical character (y_0 = 0.989) and unusual stability. Variable-temperature electron spin resonance (VT-ESR) suggests a singlet ground state and a small single-triplet gap of −0.24 kcal mol^{-1}. Density functional theory (DFT) calculations unveil that the electron-deficient phospha[5]helication has no obvious contribution to the spin delocalization via TBC, but the folded helical overlay points out a perfect overlay of two radical spots, which is quite different from the other reported carbon[*n*]helicene diradicals.[35] In contrast, the Cu(II)-mediated C−H bond cleavage and C−P bond cyclization produce complex multiple diradicals on the *P* and *N* atoms without priority. According to the control experiment on a carbazole-fused substrate, the multiple diradical mixture could contain radical phospha[6]dication and radical substrate oxides. The helical and planar D−A phosphoniums show topology symmetry-dependent optoelectronic nature, which is reflected in distinct polar-dependent electron transfer. These facts highlight the significance of SET-directed design in transient and stable radicals.

RESULTS AND DISCUSSION

Synthesis of Helical and Planar Phosphoniums. Development of this C−P bond annulation began with establishing a modified synthetic method based on our previous and Anslyn's works.[53,54] The optimized synthetic routes to phosphoniums were explored as displayed in Figures 1b and S1. The former investigation found that the C−P activation, cleavage, and annulation could be realized by *in situ* Mn(III)-mediated of simple diphosphines at ambient conditions. However, the reactions would be much harder for some complex derivatives, which is related to their limited oxidation potential and spatial construction.[53] To resolve this issue, we are inspired by the principle of oxidation enhancement

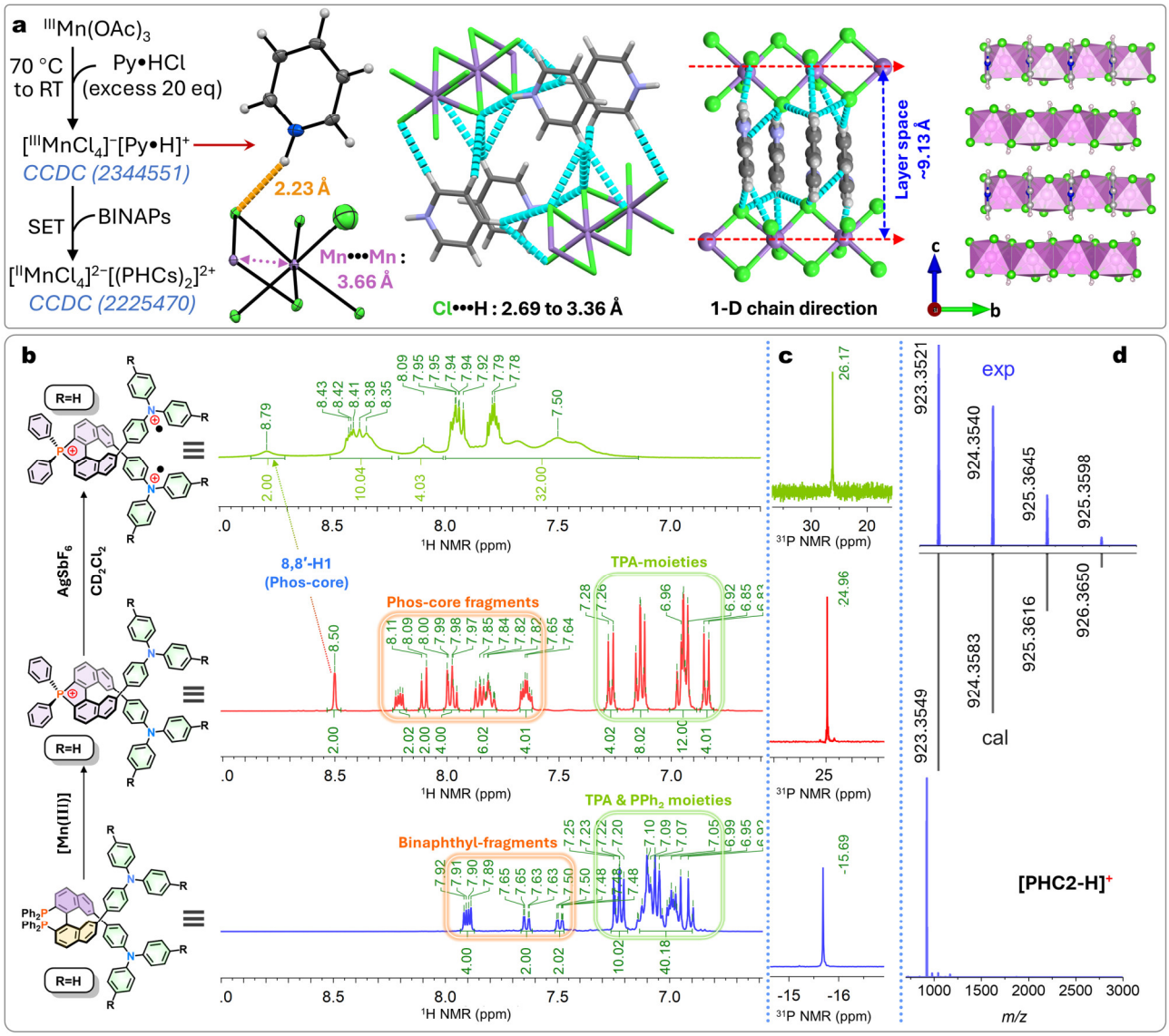

Figure 2. (a) Simulated and experimental ESI-HRMS spectra of **[PHC2-H]$^+$[Cl]$^-$**. (d) Preparative routes of **{[^{III}MnCl$_4$]$^-$[Py•H]$^+$}$_n$** and its SCXRD structures and SET efficacy for C−P activation. (b) Aromatic region of the ^{1}H NMR spectra and (c) ^{31}P NMR spectra of **P2-H** ligand, **[PHC2-H]$^+$[Cl]$^-$**, and **[PHC2-H]$^{2•3+}$[(SbF$_6$)$_3$]$^-$** (400 MHz/160 MHz, CD_2Cl_2, 25 °C). (d) HRMS spectra of **[PHC2-H]$^+$[Cl]$^-$**.

in acidic conditions,[1] and prepared several electron-rich diphosphines with substituted carbazoles (CZs) or triphenylamines (TPAs) at 7,7'-positions to implement folded helical centers after annulation. The substrates are inert for cyclization in neutral reaction mediums with $MnCl_2$ and O_2 but quickly activated in acidic conditions after adding excess pyridine hydrochloride (HCl•Py). The SET-induced annulation progress is observed by naked eyes, in which the color of reaction solution switches from colorless to red (Figure S2, video S1). Importantly, this SET takes precedence in *P*(III)-atoms instead of *N*-atoms because of the stronger electron binding of *N*-atoms based on higher electronegativity and deeper orbital depth (2*p* *versus* 3*p*-orbitals).

To reveal the inherently active species in acidic conditions, we successfully acquired the first example of stable Mn(III) halide crystals without extra pnictogen-oxide stabilization ({[^{III}MnCl$_4$]$^-$[Py•H]$^+$}$_n$) via ligand exchange in strong acidic conditions (Figure 2a). For the [^{III}MnCl$_4$]$^-$ part, the single-crystal X-ray diffraction (SCXRD) characterization of brown crystals reveals that the adjacent {^{III}MnCl$_4$} units are repeatedly linked by μ_2−Cl bridges, forming a 1-D coordination chain (Figure 2a). Given the coordination environment, the six-coordinated {MnCl$_6$} unit adopts a distorted octahedral geometry. The protonated pyridine ([Py•H]$^+$) couples with [MnCl$_4$]$^-$ via multiple H-bonding interactions (2.69 to 3.36 Å) to serve as a crucial tranquilizer for {^{III}MnCl$_4$}. This complex could directly activate the SET reaction of BINAPs, representing solid evidence for active hypervalent metal center attribution of C−P activation. It should be highlighted that an important feature of {[^{III}MnCl$_4$]$^-$[Py•H]$^+$}$_n$ is its bench-stability, which has been often hardly accessed and defined in the generation

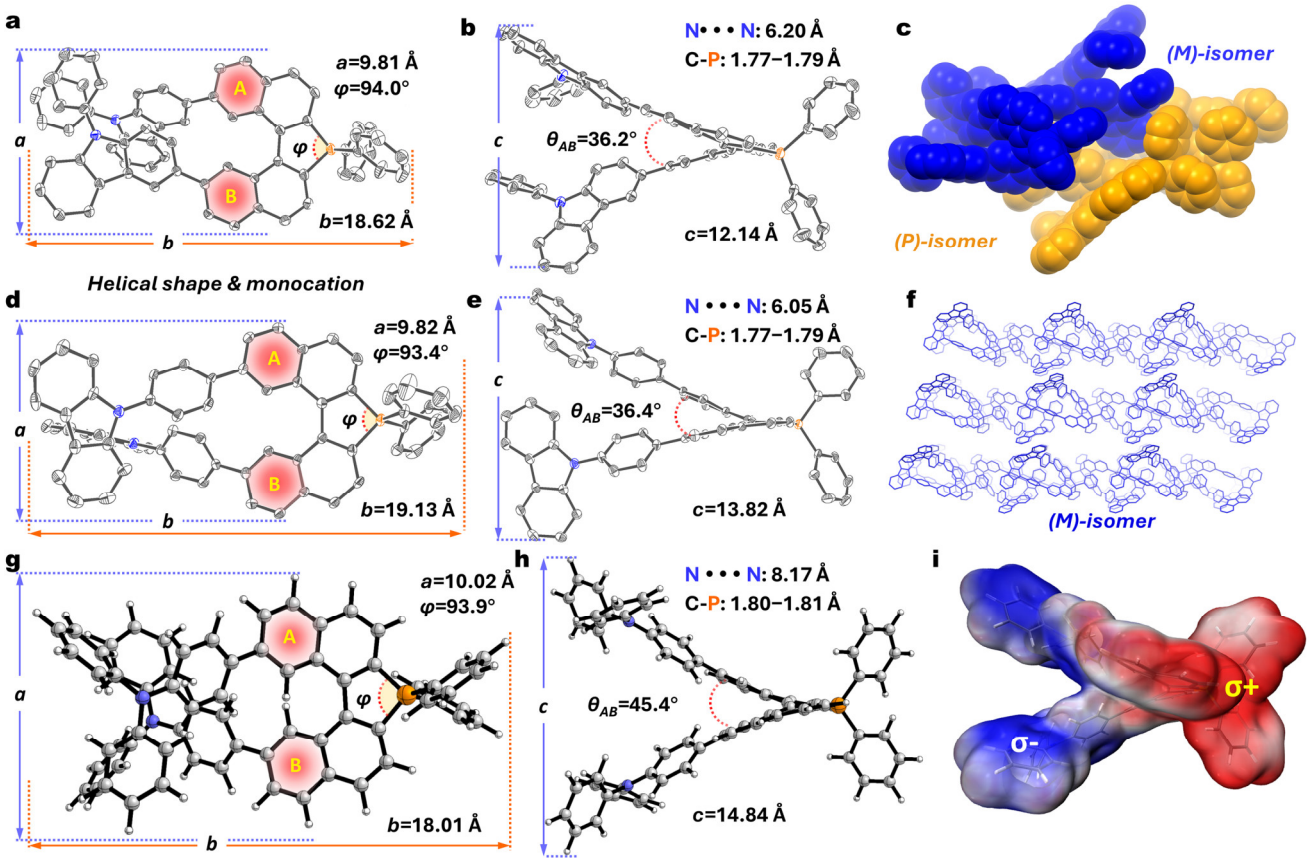

Figure 3. (a) ORTEP drawing of the crystal structure of **[PHC1]**$^{+}$**[SbF$_6$]**$^{-}$ with top view and (b) side view (thermal ellipsoids probability is 30%, anions are omitted for clarity). (c) Heterochiral packing of racemic **[PHC1]**$^{+}$**[SbF$_6$]**$^{-}$ in the unit cell. (d) ORTEP drawing of the crystal structure of **[PHC3]**$^{+}$**[SbF$_6$]**$^{-}$ with top view and (e) side view. (f) Homochiral structure arrangement of **[PHC3]**$^{+}$**[SbF$_6$]**$^{-}$ crystals. (g–h) DFT optimized molecular structure of **[PHC2-H]**$^{+}$ at the B3LYP/6-31G(d) level. (i) DFT simulated ESP mapping of **[PHC2-H]**$^{+}$ at the higher B3LYP/6-311G(d) level.

of prior {^{III}**MnCl$_3$**} methodologies.[55,56] This bench-stable complex could serve as a new SET oxidation reagent for organic synthesis and organometallic chemistry, *e.g.,* chlorination reactions[57–60] and the current C−P bond cleavage. The stark contrast between reactions in the neutral and acidic conditions for Mn(III)-mediation underlines the importance of intensified SET in permitting the emergent reactivity and regioselectivity that would otherwise be difficult to achieve. Compared with other C−P bond coupling protocols via [Pd]/[Rh]-catalysis or *de novo* synthesis,[61–66] this system represents a unique synthetic paradigm where the high activity is dependent on the formation of SET-trigged phosphonium radical between Mn(III) and phosphine moieties.[53,67,68]

Using this impressive synthetic method, five helical phosphoniums were prepared easily with acceptable yields (Figures 1, S1). On the other hand, the Cu(OTf)$_2$-mediated C−H bond activation, cleavage, and annulation were also attempted to build distinct molecular topology, resulting in corresponding planar phospha[6]dications. Unfortunately, triphenylamine-involved substrates yielded complex radical mixtures with high stability but were inseparable due to poor solubility. The ESR spectra show the persistence of multiple diradicals over one month (Figure S3a). Nonetheless, one pure phospha[6]dication of **[PDC1]**$^{2+}$**[(OTf)$_2$]**$^{2-}$ could be obtained from a carbazole-fused backbone (**P1**, Figure S1). This founding means that a new construction of novel D−A phosphoniums with distinct helical or planar geometries, such as cationic helicenes and PAHs, is possible through selectively Mn(III)/Cu(II)-mediated C−P and C−H bond cleavage.

Structural Identification and X-ray Crystal Structural Analysis. The separable compounds have been fully characterized by NMR, electrospray ionization mass spectrometry (ESI-HRMS), and SCXRD. During our study of the physicochemical properties of phosphoniums, we found that all the phosphoniums had good solubility in dichloromethane (DCM) but were insoluble in nonpolar solvents, indicating restricted aggregation in polar solvents due to nonplanar construction and polar ion pair. Phospha[5]helication **[PHC2-H]**$^{+}$**[Cl]**$^{-}$ as the typical object displays a resolvable pattern in ^{1}H NMR spectra (Figure 2b). The corresponding two individual ^{1}H domains of electron-deficientcore (20H, 8.50−7.64 ppm) and electron-rich arms (28H, 7.28−6.83 ppm) are located at the downfield and upfield respectively because of the decreased electron cloud density of electron-deficient phospha[5]helicene core. The labeled single peak of 8,8'-position protons is

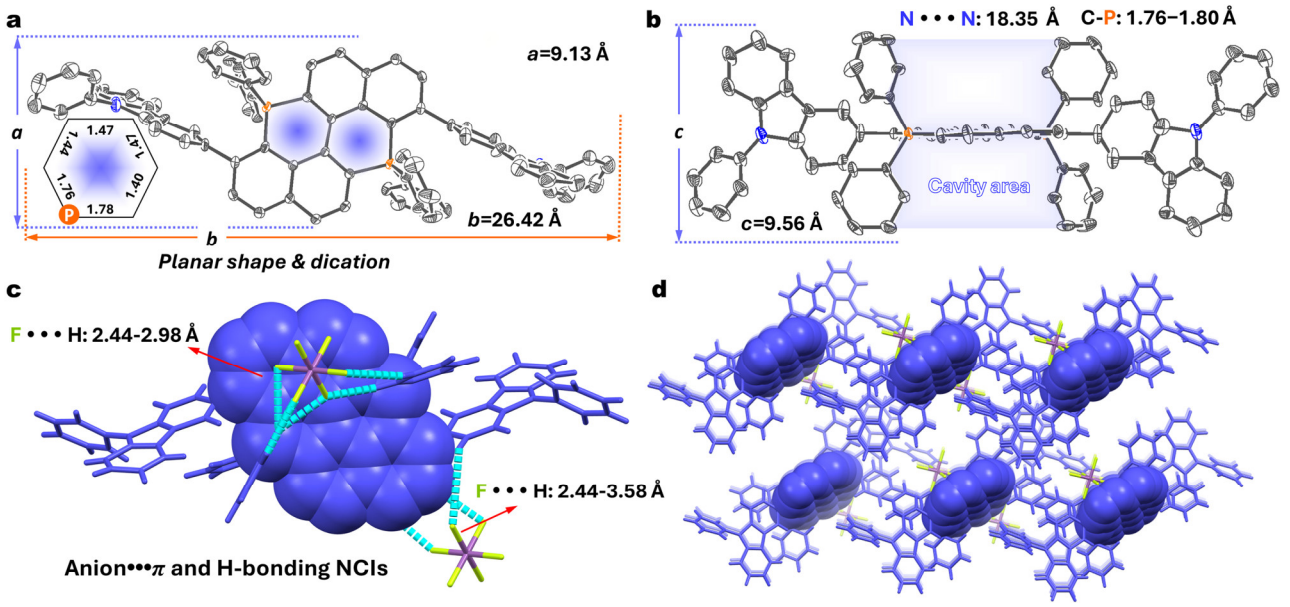

Figure 4. (a) ORTEP drawing of $[PDC1]^{2+}[(SbF_6)_2]^{2-}$ single crystals with top view and (b) side view (thermal ellipsoids probability is 30%, anions are omitted for clarity). (c) Anion•••π and H-bonding interactions analysis. (d) Crystal structure arrangement of $[PDC1]^{2+}[(SbF_6)_2]^{2-}$.

observed at 8.50 ppm. Thus, this proof is in good accordance with the C_2 symmetric helical structure of the molecule. In comparison, two individual ^{1}H domains of $[PHC2\text{-}H]^{2\cdot3+}[(SbF_6)_3]^{3-}$ are further shifted downfield as a result of the attached triarylammonium diradicals with a weak deshielding effect, which also shows extremely broadened peaks due to the presence of paramagnetic character (Figure 2b, top). Moreover, the ^{31}P NMR reveals a downfield shifting after annulation and radicalization from −15.69 to 24.96 and 26.17 ppm (Figure 2c), respectively, in line with the electron deficiency of phosphonium. The identity of $[PHC2\text{-}H]^+$ is further confirmed by ESI-HRMS with a perfect match (Figure 2d). In addition, this series of phosphoniums is quite stable for several months at ambient conditions both in the solid state and in solution.

Due to the poor crystallization of chloride counterion products, single crystals of $[PHC1]^+[SbF_6]^-$, $[PHC3]^+[SbF_6]^-$, $[PDC1]^{2+}[(SbF_6)_2]^{2-}$, and $[PDC1]^{2+}[(OTf)_2]^{2-}$ were grown in mixed DCM/PE solvents by the anion exchange (*i.e.* $AgSbF_6$ or AgOTf as Cl^- scavenger) and subsequent slow volatilization in air (Figures S4–S8). $[PHC1]^+[SbF_6]^-$ consists of a pair of (*P*) and (*M*)-enantiomers, two 4-carbazoles attached to phospha[5]helication with folded packing, where the short N•••N distance could be determined as 6.20 Å. The helical torsion is induced by C–P cyclization along with a small dihedral angle ($\theta_{A/B}$=36.2°) between adjacent naphthalenes (Figures 3a–c, S4). Similarly, the carbazole-fused $[PHC3]^+[SbF_6]^-$ displays distorted conformation as follows from the approximate N–N distance (6.05 Å) and dihedral angle (36.4°, Figures 3d–f). Interestingly, the racemic $[PHC3]^+[SbF_6]^-$ shows a chiral self-sorting via symmetry breaking, where only homogeneous (*M*)-isomers are observed in one single crystal (Figures 3f, S5). However, the single-crystal acquisition of $[PHC2\text{-}X]^+[SbF_6]^-$ is unsuccessful because of poor crystallization of *in situ* formed radicals with tricharge cations. NMR and DFT simulations point out a C_2 symmetry in $[PHC2\text{-}X]^+$, which has larger naphthalene distortion ($\theta_{A/B}$=45.4°) and N–N distance of 8.17 Å owing to nonplanar triarylamines possessing steric repulsion (Figures 3g,h). The electrostatic potential (ESP) mapping shows a positive charge and negative surfaces for phospha[5]helication and triarylamines (Figure 3i). This result manifests the character of electron-deficient phosphonium and electron-rich TPAs, in agreement with empiricism about D–A structural inference.

In contrast, $[PDC1]^{2+}[(SbF_6)_2]^{2-}$ with planar topology exhibits a deep chamber in the phospha[6]dication center, where the phospha[6]dication decorates with two 4-carbazoles and four phenyls (Figures 4a,b). This special chamber favors the anions reception capability through anion•••π (2.44–2.98 Å) and F•••H (2.44–2.58 Å) interactions at the inside and edge of a cavity with strong combinations (Figures 4c–d, S7). Remarkably, this feature has also been reproduced in other $[OTf]^-$ counterions with different anion geometric construction (2.60–2.86 Å, $[PDC1]^{2+}[(OTf)_2]^{2-}$, Figure S8), confirming that the electron-withdrawing phospha[6]dication chamber facilitates the ion-pair association in solid.

Photophysical Properties and Electronic Structures. Molecular topology-dependent electronic transfer has been fully disclosed in this class of phosphoniums in discrete unimolecular and condensed solid states. As shown in Figure 5e, HOMO and LUMO electron densities are almost discretely distributed on the helical backbone of **PHCs**, where the electron-deficient phospha[5]helicene takes the LUMO but electron-rich

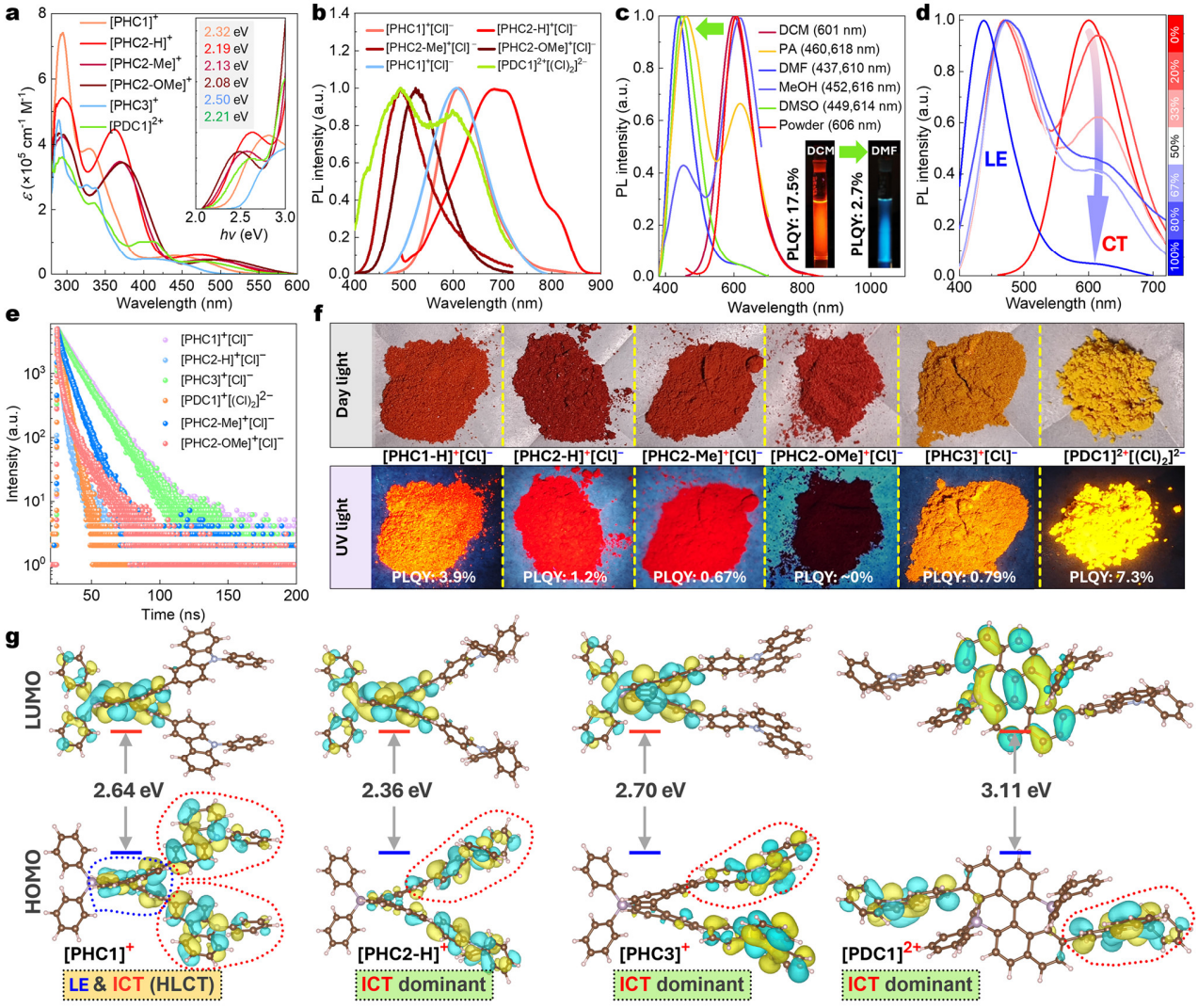

Figure 5. (a) UV−vis and (b) fluorescence spectra of Cl^- counter complexes in DCM (10^{-5} M, λ_{ex} = 370 nm). (c) Solvent-dependent PL spectra of **[PHC1]$^+$[Cl]$^-$**. (d) Solvent-ratio relevant PL spectra of **[PHC1]$^+$[Cl]$^-$** (DCM/DMF). (e) TRPL spectra of all compounds in DCM. (f) Solid emission parameters and images comparison in all compounds. (g) Orbital distribution of HOMO and LUMO for four typical cations at B3LYP/6-311G(d) level.

donor contributes the HOMO. Nevertheless, we also observed a relatively incomplete separation of HOMO−LUMO pairs in **[PHC1]$^+$**, as compared to other complexes, resulting in the helical intramolecular charge transfer (ICT) and local electronic (LE, π–π*) transition (Figures 5g, S9). This HLCT has a deep influence on the photophysical properties according to the optical observation. For instance, the five **PHCs** reveal tunable HLCT absorption from 280−600 nm, and their optical gaps are reduced from 2.50 to 2.08 eV in DCM due to enhanced donor strengths from CZs to TPAs (Figure 5a). Intriguingly, the excited HLCT is extremely sensitive to the polarity of the solvents. The fluorescence emission of **PHCs** emanates an inconsistent variation tendency in DCM and the CZ-fused **[PHC1]$^+$[Cl]$^-$** and **[PHC3]$^+$[Cl]$^-$** and displays orange emission with moderate PLQYs of 17.5 and 7.2%, respectively (Figure 5b). After the intensification of the donor, the TPA-fused **[PHC2-H]$^+$[Cl]$^-$** exhibits a red-shift emission across deep red to NIR regions (~705 nm). Unexpectedly, the blue-shift weak emission is noticed in **[PHC2-Me]$^+$[Cl]$^-$** and **[PHC2-OMe]$^+$[Cl]$^-$** after reinforcement of electron-donating capacity (Figures 5b, S10−S12), which could be related to the switchable LE and CT emission of HLCT. To unveil this appearance, the typical solvatochromism of **[PHC1]$^+$[Cl]$^-$** has been further investigated in polar solvents. **[PHC1]$^+$[Cl]$^-$** displays a negative solvatochromism effect from DCM (red emission) to DMSO (blue emission) and the emission proportion is highly influenced by polarities (Figure 5c). For example, **[PHC1]$^+$[Cl]$^-$** shows dual emission bands at ~450 (LE) and ~600 nm (CT) in acetone and methanol but a single CT/LE peak dominant in DCM, DMF, and DMSO. The intensity ratios (I_{CT}/I_{LE}) of the two peaks are decreased from 2.33 (PA) to 0.05 (DMF or DMSO) and the PLQY is highly suppressed in polar solvents. Interestingly, the ICT is gradually restrained in light of reduced I_{CT}/I_{LE} values in mixed DCM/DMF solvents with distinct ratios

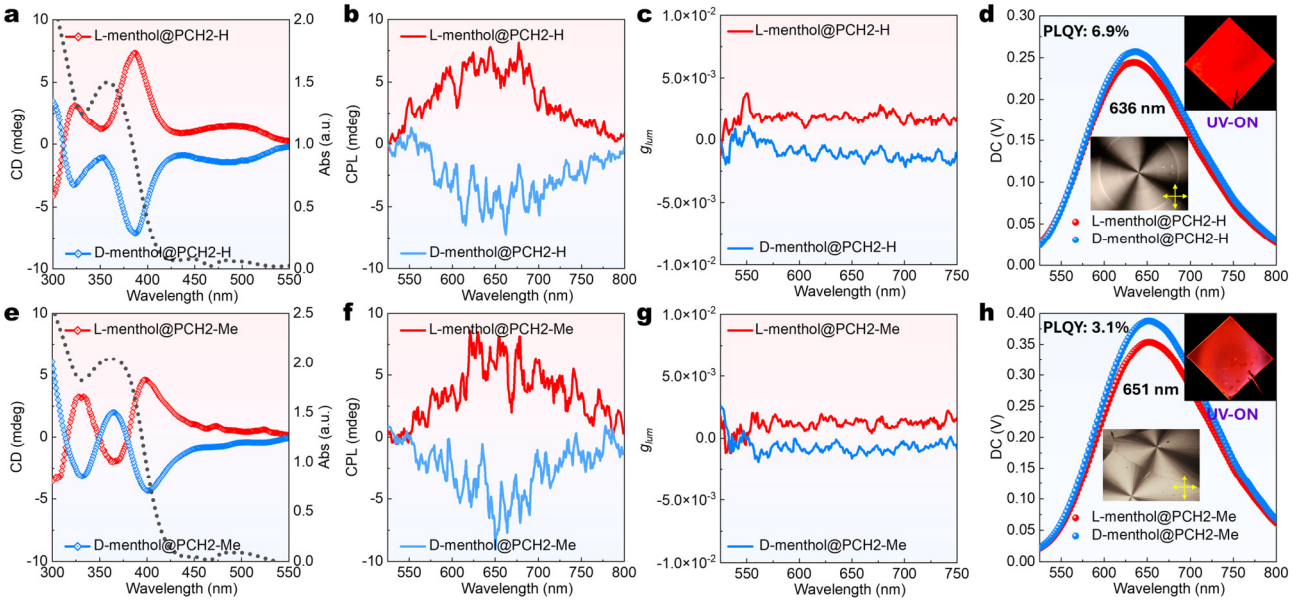

Figure 6. (a) CD and (b) CPL spectra of enantiomeric solid films for L/D-menthol@**[PCH2-H]$^+$[Cl]$^-$**. (c–d) Their corresponding g_{lum}, PL spectra, and image of the light-emitting films under 365 nm light (inserted images show polarizing microscope textures of the film). (e) CD and (f) CPL spectra of enantiomeric solid film for L/D-menthol@[**PCH2-Me]$^+$[Cl]$^-$**. (g–h) Their corresponding g_{lum}, DC spectra, and image of the light-emitting film under 365 nm light (doped with 1 wt% ratio).

(Figure 5d). Hence, the low-energy band and high-energy emission are shaped from the entire ICT and donor's LE contributions, respectively, because of altered excited state configurations.[69–71] However, other CT-dominant complexes show more sensitivity in luminescence and even emit fluorescence in DCM corresponding to the LE component (Figures 5g, S21–S23). The UV-vis and solid PL spectra reflect their intrinsic band gaps (Figures 5a, 5f, S23d). PL of solid **PHCs** possesses orange to NIR signals at 570 (**[PHC3]$^+$[Cl]$^-$**), 606 (**[PHC1]$^+$[Cl]$^-$**), 651 (**[PHC2-H]$^+$[Cl]$^-$**), and 656 nm (**[PHC2-Me]$^+$[Cl]$^-$**). The PLQY is boosted in doped PMMA for all **PHCs** and **[PDC1]$^{2+}$[(Cl)$_2$]$^{2-}$** as rigid excited states (up to 34.8%, Figure S25).

Significantly, the planar phospha[6]dication of **[PDC1]$^{2+}$[(Cl)$_2$]$^{2-}$** demonstrates the largest band gap in contrast to **PHCs**, which is consistent with HOMO–LUMO gaps from DFT simulations (Figures 5g, S13). However, only negligible solvatochromism and weak emission could be detected in distinct solvents, suggesting the presence of a nonpolar excited state (Figure S14). The dipole moment is 0 Debye, as reflected fact of reversed polar directions from two CZs to the phospha[6]dication core, but the **PHCs** endow huge dipole moments of 19.28 to 30.74 Debey (Figures S15–S19). That's why **PHCs** show polar-dependent electron transfer with excellent emission variation up to 0.78 eV (217 nm for **[PHC2-H]$^+$[Cl]$^-$**). Herein, we define a parameter $\zeta_{PET}=\Delta\lambda/\Delta P$ ($\Delta\lambda$ and ΔP stand for the emission wavelength variation and the polarity parameter variation) to quantify polar-dependent emission. The established ζ_{PET} for **[PHC1]$^+$[Cl]$^-$** **[PHC2-H]$^+$[Cl]$^-$**, and **[PHC3]$^+$[Cl]$^-$** are 54.7, 67.8, and 52.8, respectively, representing the highest records in helicenes up to now (Figure S21).[10,17,51,72,73] The carbazole-fused PHCs have longer decay kinetics (Figure 5e). These results demonstrate that the synergistic construction of a strong D–A environment by phospha[5]helication skeleton is an efficient way to prepare ultra-strong polar-dependent electron transfer materials.

Owing to the ionic superiority of these compounds, their dissolution ability has been checked in enantiomeric menthol. Only **[PHC2-H]$^+$[Cl]$^-$**, **[PHC2-Me]$^+$[Cl]$^-$**, and **[PHC2-OMe]$^+$[Cl]$^-$** could be dissolved in melting menthol because of the poor solubility of other rigid complexes. By fast quenching of mixed melts on cooling metal substrate, the solid films with strong fluorescence are facilely prepared. These films display an obvious optical activity and elevated PLQYs (up to 6.9%). The CD and CPL show mirrored spectra with moderate luminescent dissymmetry factors (g_{lum}) of 1.8×10^{-3} and -1.4×10^{-3} of the **L/D-menthol@PHC2-H** system (Figures 6a–h). The crystalline morphology with uniform distribution has been checked by a polarizing optical microscope, where the typical spherulitic crystal birefringence is observed in films (Figures 6d–h, S27).[74,75] These textures are identical to those of pure menthol melt after cooling (Figure S26), thereby allowing good compatibility and chiral induction in doped films. It is worth noting that the emission color has only a slight blue shift compared to that of solid powder. However, **PHC1** and **PDC1** are insoluble in L-menthol and no CPL could be found (Figure S28a, S28d). This result implies effective chiral induction and transfer in a chiral eutectic medium via H-bonding and polar interactions.[76,77]

Electronic Oxidation of Phosphoniums and Diradical Character. Incorporation of the helical TPAs provides an opportunity to study through-space spin-spin

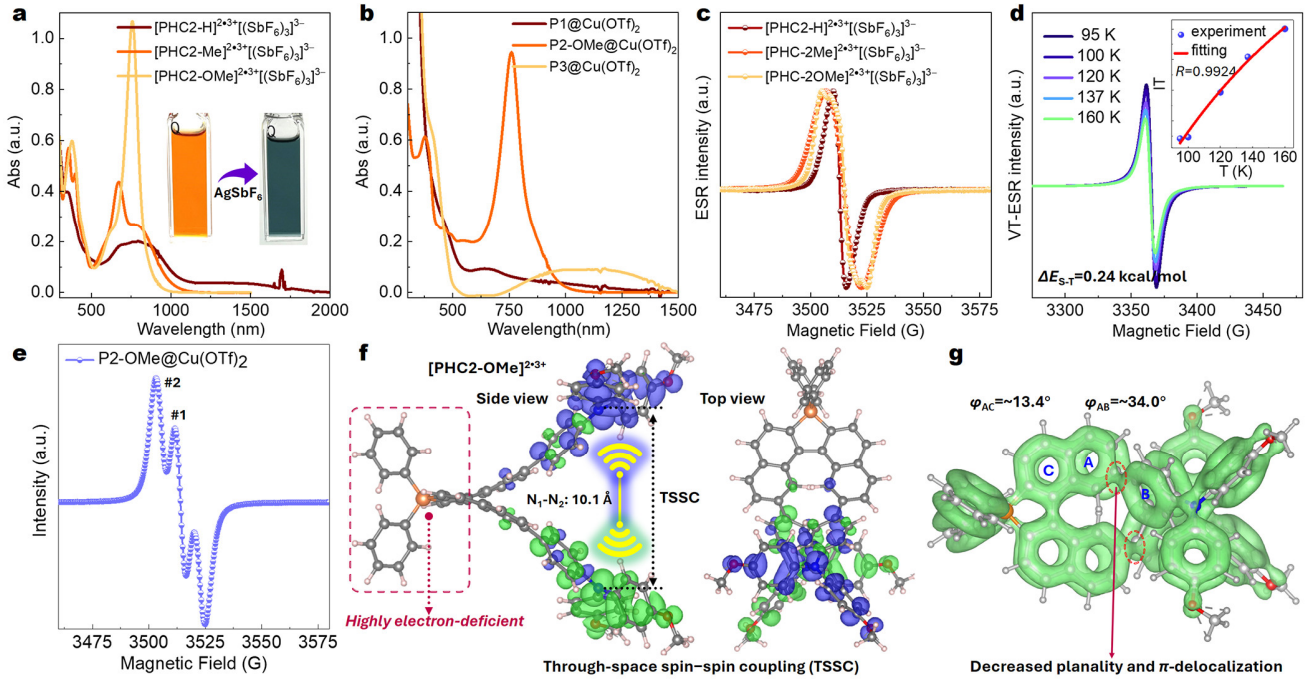

Figure 7. (a) UV−vis−NIR absorption spectra of **PHCs** radicals the DCM solution at ambient conditions (inside pictures are **[PHC2-H]$^{+}$[Cl]$^{-}$** solution before and after oxidation by 10 equiv $AgSbF_6$). (b) UV−vis−NIR absorption spectra of Cu(II)-mediated reaction solutions for **P1**−**P3** ligands at ambient conditions (V_{DCM}/V_{MeCN}=1/1). (c) ESR spectra of three radicals with excess $AgSbF_6$ (10 equiv, in DCM) at ambient conditions. (d) VT-ESR spectra of diradical **[PHC2-OMe]$^{2•3+}$[(SbF$_6$)$_3$]$^{3-}$** at cryogenic conditions by liquid N_2. (e) ESR spectra of Cu(II)-mediated reaction solutions for **P2-OMe@Cu(OTf)$_2$**. (f) Spin-density populations of diradicals **[PHC2-OMe]$^{2•3+}$[(SbF$_6$)$_3$]$^{3-}$**. (g) LOL-π isosurface of diradical **[PHC2-OMe]$^{2•3+}$**.

coupling (TSCC) for diradicals in this system. Experiments and DFT simulations have been performed to confirm this concept. As shown in Figure 7a, the orange color of the **PHC2** series in DCM is changed into dark green after the addition of excess $AgSbF_6$, where the fluorescence is also quenched rapidly. As recorded in the UV−vis−NIR spectra, the addition of $AgSbF_6$ leads to intense long-wavelength absorption bands beyond 600 nm. The **[PHC2-H]$^{2•3+}$[(SbF$_6$)$_3$]$^{3-}$** products display clear ^{1}H NMR spectra with broadened peaks but are also responsive to the ESR measurement, indicating the generation of open-shell cationic species (Figures 2b, 7c).[78] However, **[PHC2-Me]$^{2•3+}$[(SbF$_6$)$_3$]$^{3-}$** and **[PHC2-OMe]$^{2•3+}$[(SbF$_6$)$_3$]$^{3-}$** exhibit silent NMR and stronger ESR signals with broader features, suggesting that more open-shell species are formed by the chemical oxidation at *N* centers (Figures 7c, S81−S84). This multiple oxidation event has also been confirmed by cyclic voltammetry (CV, Figure S30) proofs. The broad ESR signal with no obvious hyperfine coupling indicates the formation of diradical trications. Although the compound of **[PHC2-H]$^{2•3+}$[(SbF$_6$)$_3$]$^{3-}$** does not carry substituents on TPAs, it can still be stable for more than ten hours at ambient conditions. Expectantly, the Me and OMe protected **[PHC2-Me]$^{2•3+}$[(SbF$_6$)$_3$]$^{3-}$** and **[PHC2-OMe]$^{2•3+}$[(SbF$_6$)$_3$]$^{3-}$** possess higher half-life periods over two weeks in air (Figure S3). Besides, **[PHC2-H]$^{2•3+}$[(SbF$_6$)$_3$]$^{3-}$** processes a longer wavelength absorption in NIR, NMR activity, and a narrower ESR signal, which might indicate the reservation of some doublet radicals and further oxidation frustration (*i.e.* monoradical **[PHC2-H]$^{•2+}$[(SbF$_6$)$_2$]$^{2-}$**).[17] In contrast, **[PHC2-Me]$^{2•3+}$[(SbF$_6$)$_3$]$^{3-}$** and **[PHC2-OMe]$^{2•3+}$[(SbF$_6$)$_3$]$^{3-}$** express a broader ESR peak with weak split and a higher energy absorption in UV−vis−NIR spectra, implying the generation of diradical trications with weak electronic coupling of two radicals by TSCC.[34]

To confirm this situation, the spin-unrestricted DFT calculation (UB3LYP) proofs reveal that the spin density distribution of charges in **[PHC2-OMe]$^{2•3+}$** is nearly localized in each TPA moiety with small spatial occupancy at phospha[5]helicene cation, manifesting the synergetic electron-deficient character and weak π-delocalization (Figure 7f). The calculated localized orbital locator (LOL-π) map proves the decreased planarity and π-delocalization between the phospha[5]helicene cation and TPA diradicals (Figure 7g). The spin density of diradicals is perfectly cross-folded at the helical terminals, resulting in a large space distance of 10.11 Å compared to the precursor (8.18 Å) because of the coulombic repulsion (Figure 7f).[79] The diradical character y_0 of **[PHC2-OMe]$^{2•3+}$** is calculated to be 0.989 by Yamaguchi's scheme at UB3LYP-6-311G(d) level (details see SI),[80] which surpasses the previous diradical macrocycles (y_0=0.53).[17] To confirm the diradical spin state, VT-ESR measurements are executed. The *IT (IT* stand product of ESR intensity and temperature)

intensities of **[PHC2-OMe]$^{2\bullet3+}$[(SbF$_6$)$_3$]$^{3-}$** gradually decrease with decreasing temperature from 160 to 95 K, indicating a singlet ground state of this diradical trication (Figure 7d). Further, the Bleaney-Bowers equation fitting gives a small singlet−triplet energy gap (ΔE_{S-T} = −0.24 kcal mol^{-1}).

Cu(II)-mediated C−H bond cleavage to obtain planar phospha[6]dication from **P2-OMe** leads to an unexpected stable diradical mixture ($t_{1/2}$>10 days) which can be verified by a broad and pseudo-split ESR signal with a *g* value of 2.004 (Figure 7e). In addition, the mixture has an NIR absorption up to 1100 nm, as shown in Figure 7b. According to the reaction path (Figures 1b, S36), the cyclized radical product **[PDC2-OMe]$^{2\bullet4+}$[(OTf)$_4$]$^{4+}$** and the oxidative radical product **[P2O-OMe]$^{2\bullet2+}$[(OTf)$_2$]$^{2+}$** could be responsible for the multiple radical characters. In fact, this Cu(II)-mediated annulation processes a short lifetime radical mechanism, and the trace could be found by means of the UV−vis−NIR monitor. For example, the addition of excess Cu(OTf)$_2$ leads to two new long-wavelength absorption bands up to 1500 nm (Figure 7b). Nevertheless, the separation and purification of radical **[PDC2-OMe]$^{2\bullet4+}$[(OTf)$_4$]$^{4+}$** and nonradical **[PDC3]$^{2+}$[(OTf)$_2$]$^{2-}$** are unprocurable due to poor solubility. Contrastively, the **P1** ligand suffers exclusively radicalization on the BINAP core to produce **[PDC3]$^{2+}$[(OTf)$_2$]$^{2-}$** with the planar topology. This work demonstrates the first successful construction of predominant diradicals and extremely polar-dependent electron transfer in phospha[5]helicenes via the implantation of stark D−A motifs.

CONCLUSIONS

In summary, a series of stable D−A phospha[5]helicene-based diradicals **PHCs** and phospha[6]dication-based **PDCs** are synthesized via radical-mediated topology synthesis. These *P*/*N* doped D−A helicenes show folded molecular conformation and unique photo-electro-magnetic properties that are distinct from the reported carbon[*n*]helicene analogs and traditional triarylated ammonium radicals. The tunable blue to NIR emission and chiral-induced CPL are achieved by controlling the D−A charge-transfer strength and ionic solubility. Importantly, the dynamic polar-dependent electron transfer is formed by modulating the HLCT process from topological symmetry (ζ_{PET} up to 67.8), but the symmetric **PDCs** do not have this feature. In addition, the chemical oxidative diradicals show a counterintuitive persistence with high diradical character (y_0 = 0.989). Consequently, this family of D−A phosoha[*n*]helicenes could serve as a promising platform to enforce polar diradical design and functionalization in the future.

ASSOCIATED CONTENT

Supporting Information

The Supporting Information is available free of charge at https://pubs.acs.org/doi/xxxxxx.

Experimental section; NMR and SCXRD identification of compounds; theoretical calculations; and additional figures (PDF).

Videos of the cyclization phenomenon P1 ligand under 313 K (ZIP).

Accession codes

CCDC numbers 2344545−2344549 and 2344551 contain the supplementary crystallographic data for this paper. These data can be obtained free of charge via www.ccdc.cam.ac.uk/data_request/cif, or by emailing data_request@ccdc.cam.ac.uk, or by contacting The Cambridge Crystallographic Data Centre, 12 Union Road, Cambridge CB2 1EZ, UK; fax: +44 1223 336033.

AUTHOR INFORMATION

Corresponding Author

Wei Huang − *State Key Laboratory of Coordination Chemistry, School of Chemistry and Chemical Engineering, Nanjing University, Nanjing 210093, P. R. China; Shenzhen Research Institute of Nanjing University, Shenzhen 518057, P. R. China;* orcid.org/0000-0002-1071-1055; Email: whuang@nju.edu.cn

Authors

Bo Yang − *State Key Laboratory of Coordination Chemistry, School of Chemistry and Chemical Engineering, Nanjing University, Nanjing 210093, P. R. China*

Suqiong Yan − State Key Laboratory of Coordination Chemistry, School of Chemistry and Chemical Engineering, Nanjing University, Nanjing 210093, P. R. China

Shirong Ban − *State Key Laboratory of Coordination Chemistry, School of Chemistry and Chemical Engineering, Nanjing University, Nanjing 210093, P. R. China*

Yuan Zhang − *State Key Laboratory of Coordination Chemistry, School of Chemistry and Chemical Engineering, Nanjing University, Nanjing 210093, P. R. China*

Hui Ma − *State Key Laboratory of Coordination Chemistry, School of Chemistry and Chemical Engineering, Nanjing University, Nanjing 210093, P. R. China*

Data availability statement

The data that support the findings of this study are available from ESI or the corresponding author upon reasonable request.

Conflict of interest

The authors declare no conflict of interest.

Acknowledgements

This research was supported by the National Natural Science Foundation of China (No. 21871133), the Natural Science Foundation of Jiangsu Province (No. BK20211146), and the Science, Technology, and Innovation Commission of Shenzhen Municipality (No. JCYJ20180307153251975) for financial support.

Author contributions

All authors discussed the research results and contributed to the paper.

REFERENCES

(1) Zhang, Y.; Pun, S. H.; Miao, Q. The Scholl Reaction as a Powerful Tool for Synthesis of Curved Polycyclic Aromatics. *Chem. Rev.* **2022**, *122*, 14554–14593.

(2) Anderson, H. V.; Gois, N. D.; Chalifoux, W. A. New Advances in Chiral Nanographene Chemistry. *Org. Chem. Front.* **2023**, *10*, 4167–4197.

(3) Fan, W.; Fukunaga, T. M.; Wu, S.; Han, Y.; Zhou, Q.; Wang, J.; Li, Z.; Hou, X.; Wei, H.; Ni, Y.; Isobe, H.; Wu, J. Synthesis and Chiral Resolution of a Triply Twisted Möbius Carbon Nanobelt. *Nat. Synth.* **2023**, *2*, 880–887.

(4) Ni, Y.; Gopalakrishna, T. Y.; Phan, H.; Kim, T.; Herng, T. S.; Han, Y.; Tao, T.; Ding, J.; Kim, D.; Wu, J. 3D Global Aromaticity in a Fully Conjugated Diradicaloid Cage at Different Oxidation States. *Nat. Chem.* **2020**, *12*, 242–248.

(5) May, J. H.; Van Raden, J. M.; Maust, R. L.; Zakharov, L. N.; Jasti, R. Active Template Strategy for the Preparation of π-Conjugated Interlocked Nanocarbons. *Nat. Chem.* **2023**, *15*, 170–176.

(6) Cheung, K. Y.; Watanabe, K.; Segawa, Y.; Itami, K. Synthesis of a Zigzag Carbon Nanobelt. *Nat. Chem.* **2021**, *13*, 255–259.

(7) Leonhardt, E. J.; Jasti, R. Emerging Applications of Carbon Nanohoops. *Nat. Rev. Chem.* **2019**, *3*, 672–686.

(8) Chen, J. H.; Jiang, Z. Y.; Xiao, H.; Tong, S.; Shi, T. H.; Zhu, J.; Wang, M. X. Highly Strained Oxygen-Doped Chiral Molecular Belts of the Zigzag-Type with Strong Circularly Polarized Luminescence. *Angew. Chem. Int. Ed.* **2023**, e202301782.

(9) Nishigaki, S.; Shibata, Y.; Nakajima, A.; Okajima, H.; Masumoto, Y.; Osawa, T.; Muranaka, A.; Sugiyama, H.; Horikawa, A.; Uekusa, H.; Koshino, H.; Uchiyama, M.; Sakamoto, A.; Tanaka, K. Synthesis of Belt- And Möbius-Shaped Cycloparaphenylenes by Rhodium-Catalyzed Alkyne Cyclotrimerization. *J. Am. Chem. Soc.* **2019**, *141*, 14955–14960.

(10) Jia, Y.; Li, P.; Liu, K.; Li, C.; Liu, M.; Di, J.; Wang, N.; Yin, X.; Zhang, N.; Chen, P. Expanding New Chemistry of Aza-Boracyclophanes with Unique Dipolar Structures, AIE and Redox-Active Open-Shell Characteristics. *Chem. Sci.* **2022**, *13*, 11672–11679.

(11) Segawa, Y.; Watanabe, T.; Yamanoue, K.; Kuwayama, M.; Watanabe, K.; Pirillo, J.; Hijikata, Y.; Itami, K. Synthesis of a Möbius Carbon Nanobelt. *Nat. Synth.* **2022**, *1*, 535–541.

(12) Li, C.; Shao, Y. B.; Gao, X.; Ren, Z.; Guo, C.; Li, M.; Li, X. Enantioselective Synthesis of Chiral Quinohelicenes through Sequential Organocatalyzed Povarov Reaction and Oxidative Aromatization. *Nat. Commun.* **2023**, *14*, 3380.

(13) Guo, W. C.; Zhao, W. L.; Tan, K. K.; Li, M.; Chen, C. F. B,N-Embedded Hetero[9]Helicene Toward Highly Efficient Circularly Polarized Electroluminescence. *Angew. Chem. Int. Ed.* **2024**, e202401835.

(14) Liu, Y.; Li, Z.; Wang, M. W.; Chan, J.; Liu, G.; Wang, Z.; Jiang, W. Highly Luminescent Chiral Double π-Helical Nanoribbons. *J. Am. Chem. Soc.* **2024**, *146*, 5295–5304.

(15) Tang, X.; Cui, L. S.; Li, H. C.; Gillett, A. J.; Auras, F.; Qu, Y. K.; Zhong, C.; Jones, S. T. E.; Jiang, Z. Q.; Friend, R. H.; Liao, L. S. Highly Efficient Luminescence from Space-Confined Charge-Transfer Emitters. *Nat. Mater.* **2020**, *19*, 1332–1338.

(16) Ren, L.; Han, Y.; Hou, X.; Ni, Y.; Zou, Y.; Jiao, T.; Wu, J. Aromaticity in Fully π-Conjugated Multicyclic Macrocycles. *J. Am. Chem. Soc.* **2023**, *145*, 12398–12406.

(17) Zhao, F.; Zhao, J.; Liu, H.; Wang, Y.; Duan, J.; Li, C.; Di, J.; Zhang, N.; Zheng, X.; Chen, P. Synthesis of π-Conjugated Chiral Organoborane Macrocycles with Blue to Near-Infrared Emissions and the Diradical Character of Cations. *J. Am. Chem. Soc.* **2023**, *145*, 10092–10103.

(18) Shi, Y.; Li, C.; Di, J.; Xue, Y.; Jia, Y.; Duan, J.; Hu, X.; Tian, Y.; Li, Y.; Sun, C.; Zhang, N.; Xiong, Y.; Jin, T.; Chen, P. Polycationic Open-Shell Cyclophanes: Synthesis of Electron-Rich Chiral Macrocycles, and Redox-Dependent Electronic States. *Angew. Chem. Int. Ed.* **2024**, e202402800.

(19) Huo, G. F.; Xu, W. T.; Han, Y.; Zhu, J.; Hou, X.; Fan, W.; Ni, Y.; Wu, S.; Yang, H. B.; Wu, J. Expanded Azahelicenes with Large Dissymmetry Factors. *Angew. Chem. Int. Ed.* **2024**, e202403149.

(20) Wang, P.; Xiang, Q.; Tian, M.; Tao, S.; Xu, Z.; Guo, Y.; Hu, W.; Sun, Z. Spin-Distribution-Directed Regioselective Substitution Strategy for Highly Stable Olympicenyl Radicals. *Angew. Chem. Int. Ed.* **2023**, e202313257.

(21) Shen, T.; Zou, Y.; Hou, X.; Wei, H.; Ren, L.; Jiao, L.; Wu, J. Bis-Peri-Dinaphtho-Rylenes: Facile Synthesis via Radical-Mediated Coupling Reactions and Their Distinctive Electronic Structures. *Angew. Chem. Int. Ed.* **2023**, e202311928.

(22) Jiang, Q.; Wei, H.; Hou, X.; Chi, C. Circumpentacene with Open-Shell Singlet Diradical Character. *Angew. Chem. Int. Ed.* **2023**, e202306938.

(23) Cheung, K. M.; Xiong, Y.; Pun, S. H.; Zhuo, X.; Gong, Q.; Zeng, X.; Su, S.; Miao, Q. Negatively Curved Molecular Nanocarbons Containing Multiple Heptagons Are Enabled by the Scholl Reactions of Macrocyclic Precursors. *Chem* **2023**, *9*, 2855–2868.

(24) Urieta-Mora, J.; Krug, M.; Alex, W.; Perles, J.; Fernández, I.; Molina-Ontoria, A.; Guldi, D. M.; Martín, N. Homo and Hetero Molecular 3D Nanographenes Employing a Cyclooctatetraene Scaffold. *J. Am. Chem. Soc.* **2020**, *142*, 4162–4172.

(25) Wu, S.; Ni, Y.; Han, Y.; Xin, S.; Hou, X.; Zhu, J.; Li, Z.; Wu, J. Aromaticity in Fully π-Conjugated Open-Cage Molecules. *J. Am. Chem. Soc.* **2022**, *144*, 23158–23167.

(26) Wu, S.; Ni, Y.; Han, Y.; Hou, X.; Wang, C.; Hu, W.; Wu, J. Hückel- and Baird-Type Global Aromaticity in a 3D Fully Conjugated Molecular Cage. *Angew. Chem. Int. Ed.* **2022**, e202115571.

(27) Sarkar, S. K.; Hollister, K. K.; Molino, A.; Obi, A. D.; Deng, C. L.; Tra, B. Y. E.; Stewart, B. M.; Dickie, D. A.; Wilson, D. J. D.; Gilliard, R. J. Bis(9-Boraphenanthrene) and Its Stable Biradical. *J. Am. Chem. Soc.* **2023**, *145*, 21475–21482.

(28) Dong, Y.; Sun, Z.; Xu, W.; Ma, Z.; Qiu, S.; Li, C.; Wang, H. Construction and Phosphorescence Behavior of S/Se-Heteroaromatics/Phenanthrene-Fused Hetero[9]Helicenes. *Org. Lett.* **2023**, *25*, 6715–6719.

(29) Izquierdo-García, P.; Fernández-García, J. M.; Medina Rivero, S.; Šámal, M.; Rybáček, J.; Bednárová, L.; Ramírez-Barroso, S.; Ramírez, F. J.; Rodríguez, R.; Perles, J.; García-Fresnadillo, D.; Crassous, J.; Casado, J.; Stará, I. G.; Martín, N. Helical Bilayer Nanographenes: Impact of the Helicene Length on the Structural, Electrochemical, Photophysical, and Chiroptical Properties. *J. Am. Chem. Soc.* **2023**, *145*, 11599–11610.

(30) Aribot, F.; Merle, A.; Dechambenoit, P.; Bock, H.; Artigas, A.; Vanthuyne, N.; Carissan, Y.; Hagebaum-Reignier, D.; Coquerel, Y.; Durola, F. A Triply [5]Helicene-Bridged (1,3,5)Cyclophane. *Angew. Chem. Int. Ed.* **2023**, e202304058.

(31) Toya, M.; Omine, T.; Ishiwari, F.; Saeki, A.; Ito, H.; Itami, K. Expanded [2,1][n]Carbohelicenes with 15- and 17-Benzene Rings. *J. Am. Chem. Soc.* **2023**, *145*, 11553–11565.

(32) Borissov, A.; Chmielewski, P. J.; Gómez García, C. J.; Lis, T.; Stępień, M. Dinor[7]Helicene and Beyond: Divergent Synthesis of Chiral Diradicaloids with Variable Open-Shell Character. *Angew. Chem. Int. Ed.* **2023**, e202309238.

(33) Niu, W.; Fu, Y.; Deng, Q.; Qiu, Z.-L.; Liu, F.; Popov, A. A.; Komber, H.; Ma, J.; Feng, X. Enhancing Chiroptical Responses in Helical Nanographenes via Geometric Engineering of Double [7]Helicenes. *Angew. Chem. Int. Ed.* **2024**, e202319874.

(34) Wu, H.; Hanayama, H.; Coehlo, M.; Gu, Y.; Wu, Z. H.; Takebayashi, S.; Jakob, G.; Vasylevskyi, S.; Schollmeyer, D.; Kläui, M.; Pieters, G.; Baumgarten, M.; Müllen, K.; Narita, A.; Qiu, Z. Stable π-Extended Thio[7]Helicene-Based Diradical with Predominant Through-Space Spin-Spin Coupling. *J. Am. Chem. Soc.* **2024**, *146*, 7480–7486.

(35) Hsieh, Y. C.; Wu, C. F.; Chen, Y. T.; Fang, C. Te; Wang, C. S.; Li, C. H.; Chen, L. Y.; Cheng, M. J.; Chueh, C. C.; Chou, P. T.; Wu, Y. T. 5,14-Diaryldiindeno[2,1-f:1′,2′-j]Picene: A New Stable [7]Helicene with a Partial Biradical Character. *J. Am. Chem. Soc.* **2018**, *140*, 14357–14366.

(36) Dhbaibi, K.; Favereau, L.; Crassous, J. Enantioenriched Helicenes and Helicenoids Containing Main-Group Elements (B, Si, N, P). *Chem. Rev.* **2019**, *119*, 8846–8953.

(37) Crassous, J. Chiral Transfer in Coordination Complexes: Towards Molecular Materials. *Chem. Soc. Rev.* **2009**, *38*, 830–845.

(38) Shu, C.; Zhang, H.; Olankitwanit, A.; Rajca, S.; Rajca, A. High-Spin Diradical Dication of Chiral π-Conjugated Double Helical Molecule. *J. Am. Chem. Soc.* **2019**, *141*, 17287–17294.

(39) Gan, F.; Shen, C.; Cui, W.; Qiu, H. [1,4]Diazocine-Embedded Electron-Rich Nanographenes with Cooperatively Dynamic Skeletons. *J. Am. Chem. Soc.* **2023**, *145*, 5952–5959.

(40) Tian, X.; Shoyama, K.; Mahlmeister, B.; Brust, F.; Stolte, M.; Würthner, F. Naphthalimide-Annulated [n]Helicenes: Red Circularly Polarized Light Emitters. *J. Am. Chem. Soc.* **2023**, *145*, 9886–9894.

(41) Rodríguez, R.; Naranjo, C.; Kumar, A.; Matozzo, P.; Das, T. K.; Zhu, Q.; Vanthuyne, N.; Gómez, R.; Naaman, R.; Sánchez, L.;

Crassous, J. Mutual Monomer Orientation to Bias the Supramolecular Polymerization of [6]Helicenes and the Resulting Circularly Polarized Light and Spin Filtering Properties. *J. Am. Chem. Soc.* **2022**, *144*, 7709–7719.

(42) Kiran, V.; Mathew, S. P.; Cohen, S. R.; Hernández Delgado, I.; Lacour, J.; Naaman, R. Helicenes - A New Class of Organic Spin Filter. *Adv. Mater.* **2016**, *28*, 1957–1962.

(43) Han, H.; Zhang, D.; Zhu, Z.; Wei, R.; Xiao, X.; Wang, X.; Liu, Y.; Ma, Y.; Zhao, D. Aromatic Stacking Mediated Spin-Spin Coupling in Cyclophane-Assembled Diradicals. *J. Am. Chem. Soc.* **2021**, *143*, 17690–17700.

(44) Zhu, Z.; Zhang, D.; Xiao, T.; Fang, Y. H.; Xiao, X.; Wang, X. G.; Jiang, S. Da; Zhao, D. Rational Design of an Air-Stable, High-Spin Diradical with Diazapyrene. *Angew. Chem. Int. Ed.* **2023**, *62*.

(45) Yang, X.; Zhang, D.; Liao, Y.; Zhao, D. Toward an Air-Stable Triradical with Strong Spin Coupling: Synthesis of Substituted Truxene-5,10,15-Triyl. *J. Org. Chem.* **2020**, *85*, 5761–5770.

(46) Punzi, A.; Dai, Y.; Dibenedetto, C. N.; Mesto, E.; Schingaro, E.; Ullrich, T.; Striccoli, M.; Guldi, D. M.; Negri, F.; Farinola, G. M.; Blasi, D. Dark State of the Thiele Hydrocarbon: Efficient Solvatochromic Emission from a Nonpolar Centrosymmetric Singlet Diradicaloid. *J. Am. Chem. Soc.* **2023**, *145*, 20229–20241.

(47) Fabri, B.; Funaioli, T.; Frédéric, L.; Elsner, C.; Bordignon, E.; Zinna, F.; Di Bari, L.; Pescitelli, G.; Lacour, J. Triple Para-Functionalized Cations and Neutral Radicals of Enantiopure Diaza[4]Helicenes. *J. Am. Chem. Soc.* **2024**, *146*, 8308–8319.

(48) Yang, B.; Yan, S.; Zhang, Y.; Ban, S.; Ma, H.; Feng, F.; Huang, W. Double-Model Decay Strategy Integrating Persistent Photogenic Radicaloids with Dynamic Circularly Polarized Doublet Radiance and Triplet Afterglow. *J. Am. Chem. Soc.* **2024**, *146*, 7668−7678.

(49) Zheng, X.; Huang, R.; Zhong, C.; Xie, G.; Ning, W.; Huang, M.; Ni, F.; Dias, F. B.; Yang, C. Achieving 21% External Quantum Efficiency for Nondoped Solution-Processed Sky-Blue Thermally Activated Delayed Fluorescence OLEDs by Means of Multi-(Donor/Acceptor) Emitter with Through-Space/-Bond Charge Transfer. *Adv. Sci.* **2020**, *7*, 1902087.

(50) Xin, Y.; Zhu, Y.; Chi, R.; Duan, C.; Yan, P.; Han, C.; Xu, H. Phosphine-Oxide-Balanced Intra- and Interchain Through-Space Charge Transfer in Thermally Activated Delayed Fluorescence Polymers: Beyond 30% External Quantum Efficiency. *Adv. Mater.* **2023**, *35*, 2304103.

(51) Qu, C.; Zhu, Y.; Liang, L.; Ye, K.; Zhang, Y.; Zhang, H.; Zhang, Z.; Duan, L.; Wang, Y. Helically Chiral Donor–Acceptor Double Hetero[4]Helicenes with Circularly Polarized Thermally Activated Delayed Fluorescence. *Adv. Opt. Mater.* **2023**, *11*, 2203030.

(52) Meng, G.; Zhou, J.; Han, X. S.; Zhao, W.; Zhang, Y.; Li, M.; Chen, C. F.; Zhang, D.; Duan, L. B-N Covalent Bond Embedded Double Hetero-[n]Helicenes for Pure Red Narrowband Circularly Polarized Electroluminescence with High Efficiency and Stability. *Adv. Mater.* **2024**, *36*, 2307420.

(53) Yang, B.; Yan, S.; Li, C.; Ma, H.; Feng, F.; Zhang, Y.; Huang, W. Mn(III)-Mediated C–P Bond Activation of Diphosphines: Toward a Highly Emissive Phosphahelicene Cation Scaffold and Modulated Circularly Polarized Luminescence. *Chem. Sci.,* **2023**, *14*, 10446-10457.

(54) Nieto, S.; Metola, P.; Lynch, V. M.; Anslyn, E. V. Synthesis of a Novel Bisphosphonium Salt Based on 2,2′-Bis(Diphenylphosphino)-1,1′-Binaphthyl (Binap). *Organometallics* **2008**, *27*, 3608–3610.

(55) Nachtigall, O.; Pataki, A.; Molski, M.; Lentz, D.; Spandl, J. Solvates of Manganese Trichloride Revisited - Synthesis, Isolation, and Crystal Structure of MnCl3(THF)3. *Zeitschrift fur Anorg. und Allg. Chemie* **2015**, *641*, 1164–1168.

(56) Wieghardt, K.; Bossek, U.; Nuber, B.; Weiss, J.; Bonvoisin, J. .; Corbella, M.; Vitols, S. E.; Girerd, J. J. Synthesis, Crystal Structures, Reactivity, Andmagnetochemistry of a Series of Binuclear Complexes of Manganese(II), -(III), and -(IV) of Biological Relevance. The Crystal Structure of [LMn IV(μ-O)3MnIVL](PF6)2•H2O Containing an Unprecedented Short Mn···Mn. *J. Am. Chem. Soc.* **1988**, *110*, 7398–7411.

(57) Saju, A.; Crawley, M. R.; Macmillan, S. N.; Lacy, D. C. Manganese (III) Nitrate Complexes as Bench-Stable Powerful Oxidants. *J. Am. Chem. Soc.* **2024**, https://doi.org/10.1021/jacs.4c03411.

(58) Saju, A.; Griffiths, J. R.; MacMillan, S. N.; Lacy, D. C. Synthesis of a Bench-Stable Manganese(III) Chloride Compound: Coordination Chemistry and Alkene Dichlorination. *J. Am. Chem. Soc.* **2022**, *144*, 16761–16766.

(59) Saju, A.; Gunasekera, P. S.; Morgante, P.; MacMillan, S. N.; Autschbach, J.; Lacy, D. C. Experimental and Computational Determination of a M-Cl Homolytic Bond Dissociation Free Energy: Mn(III)Cl-Mediated C-H Cleavage and Chlorination. *J. Am. Chem. Soc.* **2023**, *145*, 13384–13391.

(60) Jeong, D.; Lee, Y.; Lee, Y.; Kim, K.; Cho, J. Synthesis, Characterization, and Reactivity of a Highly Oxidative Mononuclear Manganese(IV)-Bis(Fluoro) Complex. *J. Am. Chem. Soc.* **2024**, *146*, 4172–4177.

(61) Qiu, X.; Wang, M.; Zhao, Y.; Shi, Z. Rhodium (I)-Catalyzed Tertiary Phosphine Directed C− H Arylation: Rapid Construction of Ligand Libraries. *Angew. Chem. Int. Ed.* **2017**, *56*, 7233–7237.

(62) Lian, Z.; Bhawal, B. N.; Yu, P.; Morandi, B. Palladium-Catalyzed Carbon-Sulfur or Carbon-Phosphorus Bond Metathesis by Reversible Arylation. *Science* **2017**, *356*, 1059–1063.

(63) Pang, L.; Huang, Z.; Sun, Q.; Li, G.; Liu, J.; Li, B.; Ma, C.; Guo, J.; Yao, C.; Yu, J.; Li, Q. Diversity-Oriented Synthesis of P-Stereogenic and Axially Chiral Monodentate Biaryl Phosphines Enabled by C-P Bond Cleavage. *Nat. Commun.* **2023**, *14*, 4437.

(64) Pang, L.; Sun, Q.; Huang, Z.; Li, G.; Liu, J.; Guo, J.; Yao, C.; Yu, J.; Li, Q. Palladium-Catalyzed Stereoselective Cleavage of C−P Bond: Enantioselective Construction of Atropisomers Containing a P-Stereogenic Center. *Angew. Chem. Int. Ed.* **2022**, *61*.

(65) Wang, D.; Li, M.; Shuang, C.; Liang, Y.; Zhao, Y.; Wang, M.; Shi, Z. Rhodium-Catalyzed Selective Direct Arylation of Phosphines with Aryl Bromides. *Nat. Commun.* **2022**, *13*, 1–10.

(66) Zhang, F. P.; Wang, R. H.; Li, J. F.; Chen, H.; Hari Babu, M.; Ye, M. Intermolecular Carbophosphination of Alkynes with Phosphole Oxides via Ni−Al Bimetal-Catalyzed C−P Bond Activation. *Angew. Chem. Int. Ed.* **2023**, *62*, e202314701.

(67) Liu, L.; Li, L.; Wang, X.; Sun, R.; Zhou, M. D.; Wang, H. Mn(III)-Mediated Radical Cyclization of o-Alkenyl Aromatic Isocyanides with Boronic Acids: Access to N-Unprotected 2-Aryl-3-Cyanoindoles. *Org. Lett.* **2021**, *23*, 5826–5830.

(68) König, N.; Godínez-Loyola, Y.; Weiske, H.; Naumov, S.; Lönnecke, P.; Tonner-Zech, R.; Strassert, C. A.; Hey-Hawkins, E. Access to Strong Thieno[3,2-b]Phosphole-Based Solid-State Emitters via Manganese(III)-Mediated Oxidative Annulation. *Chem. Mater.* **2023**, *35*, 8218–8228.

(69) Tang, X.; Bai, Q.; Peng, Q.; Gao, Y.; Li, J.; Liu, Y.; Yao, L.; Lu, P.; Yang, B.; Ma, Y. Efficient Deep Blue Electroluminescence with an External Quantum Efficiency of 6.8% and CIEy < 0.08 Based on a Phenanthroimidazole-Sulfone Hybrid Donor-Acceptor Molecule. *Chem. Mater.* **2015**, *27*, 7050–7057.

(70) Wang, Y.; Guo, Z.; Gao, Y.; Tian, Y.; Deng, Y.; Ma, X.; Yang, W. Tuning Hybridized Local and Charge-Transfer Mixing for Efficient Hot-Exciton Emission with Improved Color Purity. *J. Phys. Chem. Lett.* **2022**, *13*, 6664–6673.

(71) Zhong, Z.; Zhu, X.; Wang, X.; Zheng, Y.; Geng, S.; Zhou, Z.; Feng, X. J.; Zhao, Z.; Lu, H. High Steric-Hindrance Windmill-Type Molecules for Efficient Ultraviolet to Pure-Blue Organic Light-Emitting Diodes via Hybridized Local and Charge-Transfer Excited-State. *Adv. Funct. Mater.* **2022**, *32*, 2112969.

(72) Liu, J.; He, T.; Gong, Z. L.; Liang, N.; Feng, Y.; Long, G.; Zhong, Y. W.; Yao, C. J. Rational Design of Circularly Polarized Luminescent Molecular Structures Toward NIR and Single Molecule White Light Emission. *Adv. Opt. Mater.* **2023**, *23*, 2302486.

(73) Peng, L. J.; Wang, X. Y.; Li, Z. A.; Gong, H. Y. All Carbon Helicenes and π-Extended Helicene Derivatives. *Asian J. Org. Chem.* **2023**, *12*, e202300543.

(74) Walton, F.; Bolling, J.; Farrell, A.; MacEwen, J.; Syme, C. D.; Jiménez, M. G.; Senn, H. M.; Wilson, C.; Cinque, G.; Wynne, K. Polyamorphism Mirrors Polymorphism in the Liquid-Liquid Transition of a Molecular Liquid. *J. Am. Chem. Soc.* **2020**, *142*, 7591–7597.

(75) Kovács, T.; Szücs, R.; Holló, G.; Zuba, Z.; Molnár, J.; Christenson, H. K.; Lagzi, I. Self-Assembly of Chiral Menthol Molecules from a Liquid Film into Ring-Banded Spherulites. *Cryst. Growth Des.* **2019**, *19*, 4063–4069.

(76) Wen, X.; Du, S.; Zhang, L.; Liu, M. Chiral Deep Eutectic Solvents Enable Full-Color and White Circularly Polarized Luminescence

from Achiral Luminophores. *Angew. Chem. Int. Ed.* **2023**, *62*, e202311816.
(77) Bai, X.; Sun, Y.; Jiang, Y.; Zhao, G.; Jiang, J.; Yuan, C.; Liu, M. Circularly Polarized Luminescence from Solvent-Free Chiral Organic π-Liquids. *Angew. Chem. Int. Ed.* **2021**, *60*, 3745–3751.
(78) Abe, M. Diradicals. *Chem. Rev.* **2013**, *113*, 7011−7088.
(79) Grimme, S.; Djukic, J. P. Cation-Cation "Attraction": When London Dispersion Attraction Wins over Coulomb Repulsion. *Inorg. Chem.* **2011**, *50*, 2619–2628.
(80) Yamaguchi, K. The Electronic Structures of Biradicals in the Unrestricted Hartree-Fock Approximation. *Chem. Phys. Lett.* **1975**, *33*, 330–335.

TOC: *Strong D–A conjugated phosphoniums of **PHCs** and **PDCs** have been described firstly using the radical-directive topology synthesis, which contain phospha[5]helication and phospha[6]dication species. In this paper, an atomically precise Mn(III) halide has been unprecedentedly captured and determined for the C−P bond activation. These D−A pairs show unique topology dependence on the optoelectronic properties due to the dissymmetry of molecular polarity, i.e. extreme HLCT-induced solvatochromic luminescence ($\Delta\lambda_{em}$ up to 0.78 eV), co-assembly driven CPL (g_{lum} up to 1.8 × 10^{-3}), and high diradical character (y_0 = 0.989).*